

Atmosphere and ionosphere responses to infrasonic acoustic waves driven by the 2016 Kaikōura earthquake

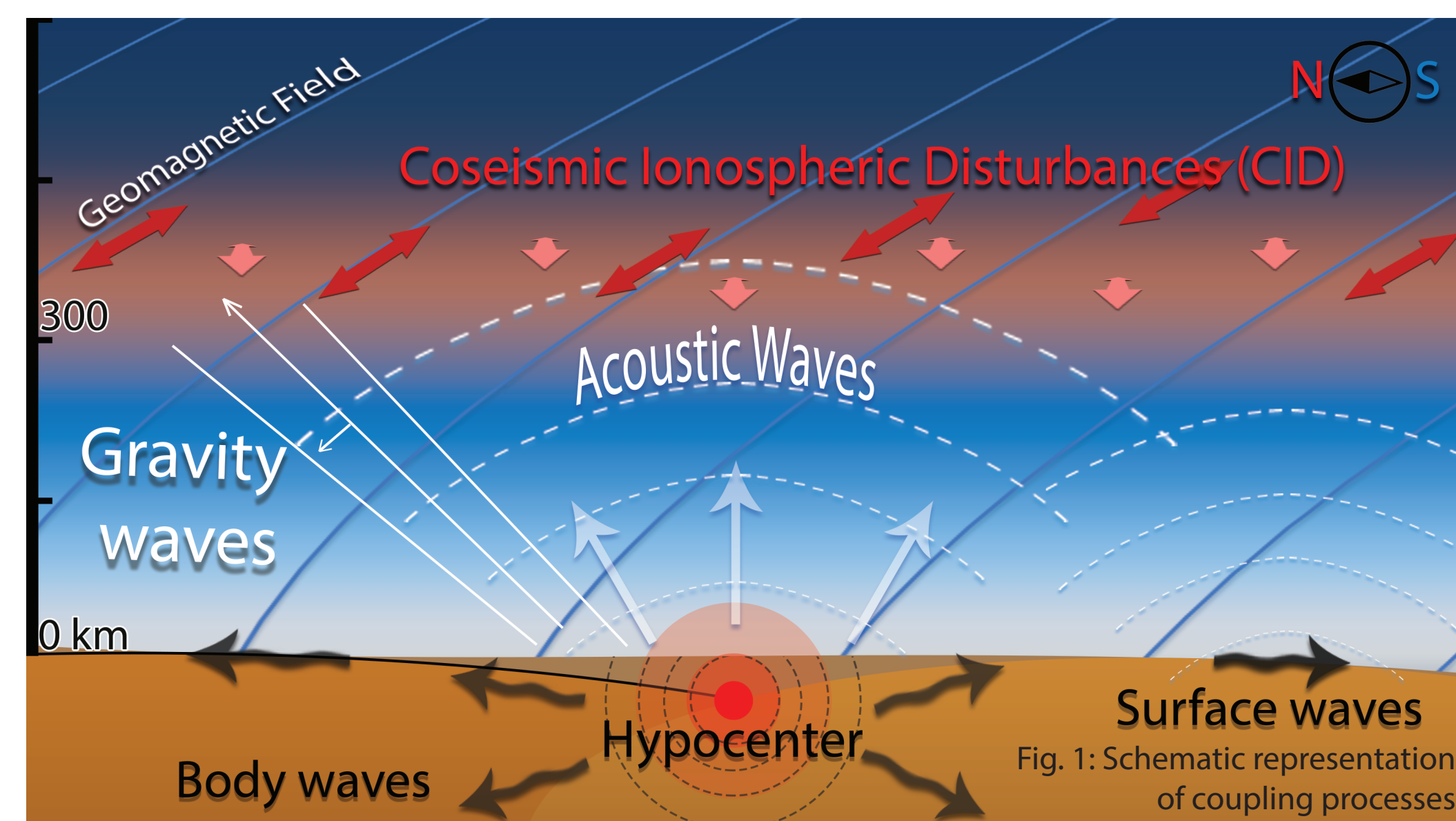
P.A. Inchin,⁽¹⁾ J.B. Snively,⁽¹⁾ Y. Kaneko,⁽²⁾ M.D. Zettergren,⁽¹⁾ A. Komjathy,⁽³⁾ O. Verkhoglyadova⁽³⁾



(1) Embry-Riddle Aeronautical University, Daytona Beach, FL, USA
 (2) GNS Science, New Zealand
 (3) Jet Propulsion Laboratory, California Institute of Technology, Pasadena, CA, USA
 E-mail: inchin@my.erau.edu

Abstract and Importance of Research

Natural hazards serve as a source of disturbances to the solid (earthquakes, landslides), liquid (tsunamis) or gaseous (tornados, hurricanes, volcanic eruptions) envelopes of the Earth. As they couple with the atmosphere, these disturbances can drive acoustic and gravity waves (AGWs) that propagate to the upper atmosphere. Due to the conservation of energy, the decrease of density in the atmosphere with altitude results in exponential growth of these waves, triggering coseismic ionospheric disturbances (CID) in the overlying ionosphere and perturbations in mesosphere airglow, which can be observed using in-situ or remote sensing instruments. Such observations can help to improve the understanding of coupling processes, supplement seismological studies and, for example, early-warning tsunami systems. However, ground- and space-based observations suffer from low spatial and temporal resolution and other instrumentation challenges. Numerical simulations are an important and necessary step for deeper understanding of coupling processes, as well as understanding how we can observe them.



Here, we present numerical simulation results of AWs dynamics and driven mesospheric airglow and ionospheric plasma responses during the 2016 Kaikōura Mw 7.8 earthquake in New Zealand. Nighttime occurrence of this event is interesting from the perspective that the background electron density is fairly small. Also, the earthquake exhibited unusual complexity of multi-segmented rupturing processes and, still, several aspects of faulting mechanism are unclear for seismologists (Hamling et al., 2017). Atmospheric and ionospheric observations could provide additional insight into some of these processes and this study is partially devoted to the possibility to describe earthquake processes by investigating the coupling of their dynamics with upper atmosphere and ionosphere.

Modeling Approach

To simulate realistic responses, we combine three numerical models spanning from the Earth's surface, to its atmosphere, and ionosphere. The seismic wave propagation codes SPEC3D (Komatitsch and Vilotte, BSSA, 1998; Komatitsch and Tromp, GJI, 149, 2002) combined with kinematic slip models are used to simulate surface displacements time-dependently. These surface displacements are then used to drive the 3D MAGIC model as the time-dependent lower-boundary conditions. 3D neutral atmosphere model MAGIC (domain shown as a cube) is used to simulate atmospheric dynamics, acoustic and gravity wave generation, propagation, and dissipation (Snively, GRL, 2013). Then, we do a slice along longitude of interest from 3D MAGIC simulation and use it as an input to 2D GEMINI model (tilted dipole) which encapsulates the ionospheric response to neutral forcing through neutral drag, dynamo currents, and modifications to thermospheric densities (Zettergren and Semeter, JGR, 2012). The coupled MAGIC-GEMINI model enables realistic simulation of atmosphere-ionosphere responses to ground-based and tropospheric perturbations (Zettergren and Snively, JGR, 2015; Zettergren et al., JGR, 2017). Results show the complexity of earthquake-atmosphere-ionosphere coupling and motivate further investigations of this interconnection and resulting observable signatures.

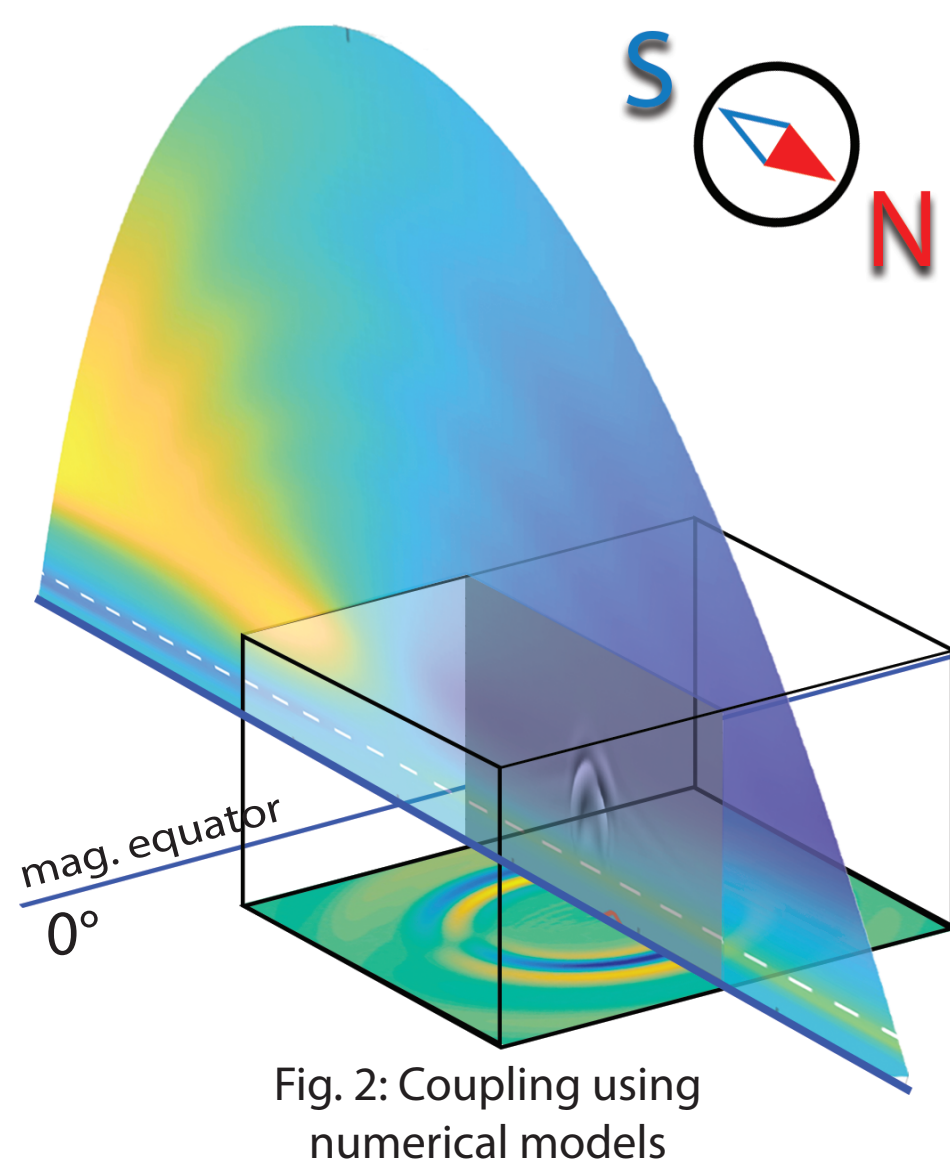


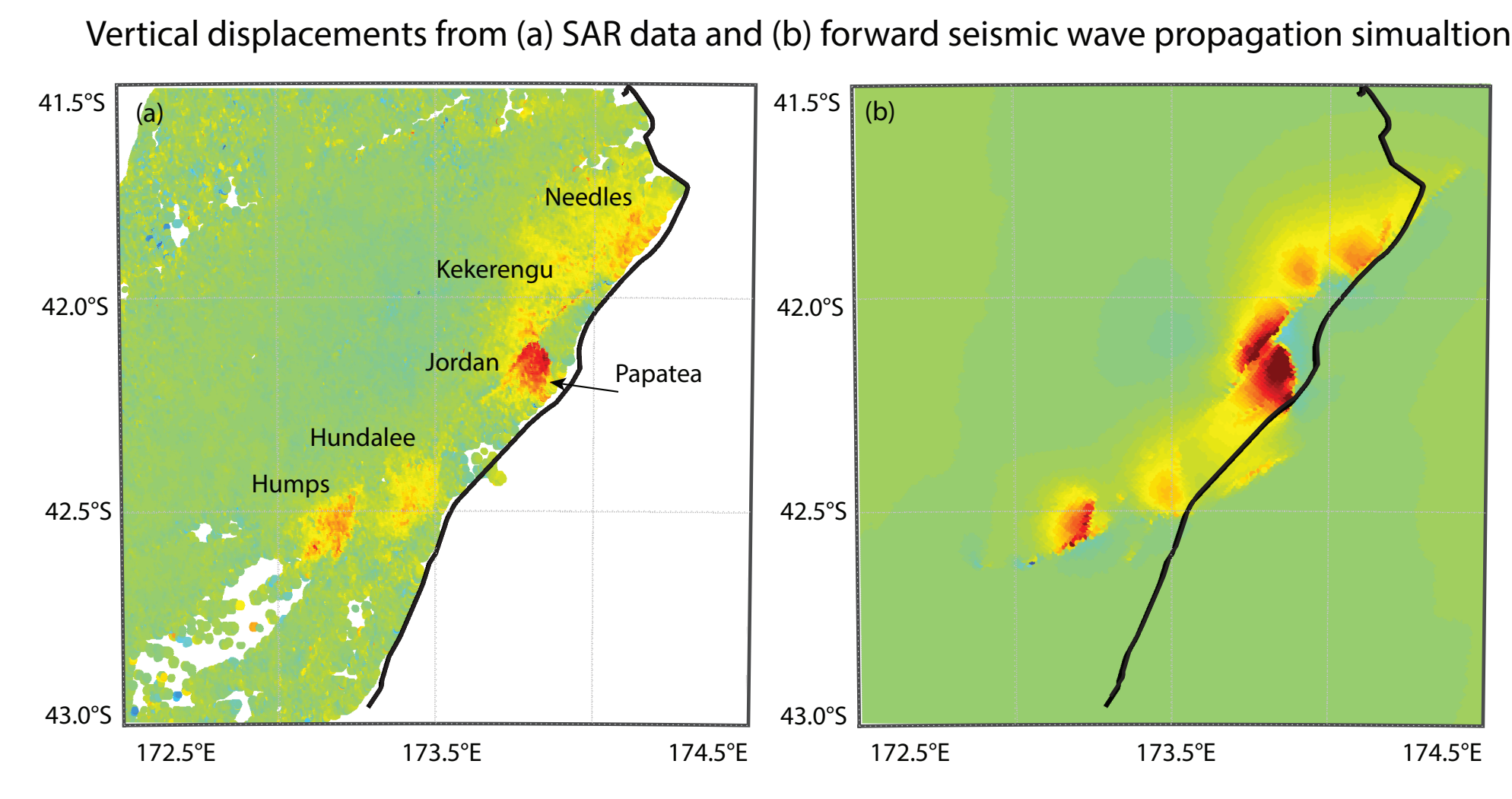
Fig. 2: Coupling using numerical models

Earthquake Description

New Zealand is situated in a tectonically complex region representing transition from Hikurangi subduction zone at north-east to strike-slip dominating Alpine fault zone in South Island. The earthquake happened in South Island in the region of Marlborough fault system (Table 1). Field observations revealed ground surface ruptures at ~12 faults (Hamling et al., 2017; Xu et al., 2018). Observational and modeling results suggest that the rupture nucleated at Humps fault and propagated roughly to northeast in Hundalee fault and Kean fault, offshore Kaikōura for ~50 s and then at northern source region, on Papatea (where the maximum vertical displacements were registered), Kekerengu, Jordan and finally Needles faults. Largest surface displacements (6-8 m) were found on Papatea fault, but the absence of appropriate data around the fault prevents one to accurately isolate the contribution for it to local displacements waveforms (Holden et al., 2017). Focal area length was ~150 km and the dynamics took ~100 sec.

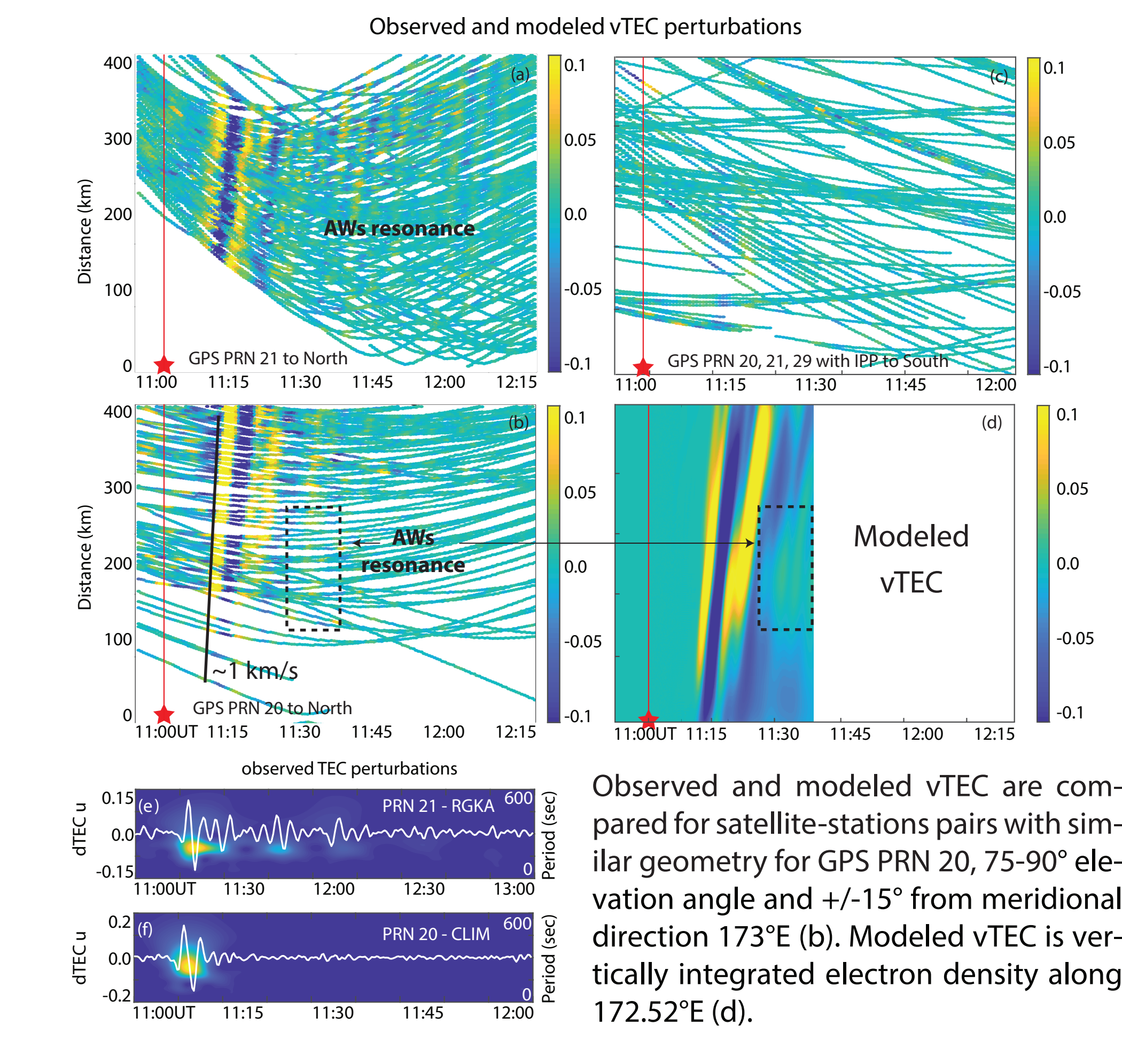
Table 1. 2016 Kaikōura earthquake	
Origin time	13.11.2016 11:02:56UTC (00:02:56LT +1)
Magnitude	7.8Mw
Epicenter	42.76°S / 173.08°E
Strike/Dip/Slip	~219°/38°/128°
Depth	~15.1 km

The kinematic slip model of Holden et al. (2017) that fits local strong-motion accelerometer and high-rate GPS data is used to model the realistic time- and spatial-dependent surface displacements. Initial model was improved with faulting characterization on Papatea fault, as discussed in (Xu et al., 2018). This kinematic source model captures a complex pattern of rupturing process from the south to north, including rupture reactivation on the Kekerengu fault 60 seconds after the origin time.



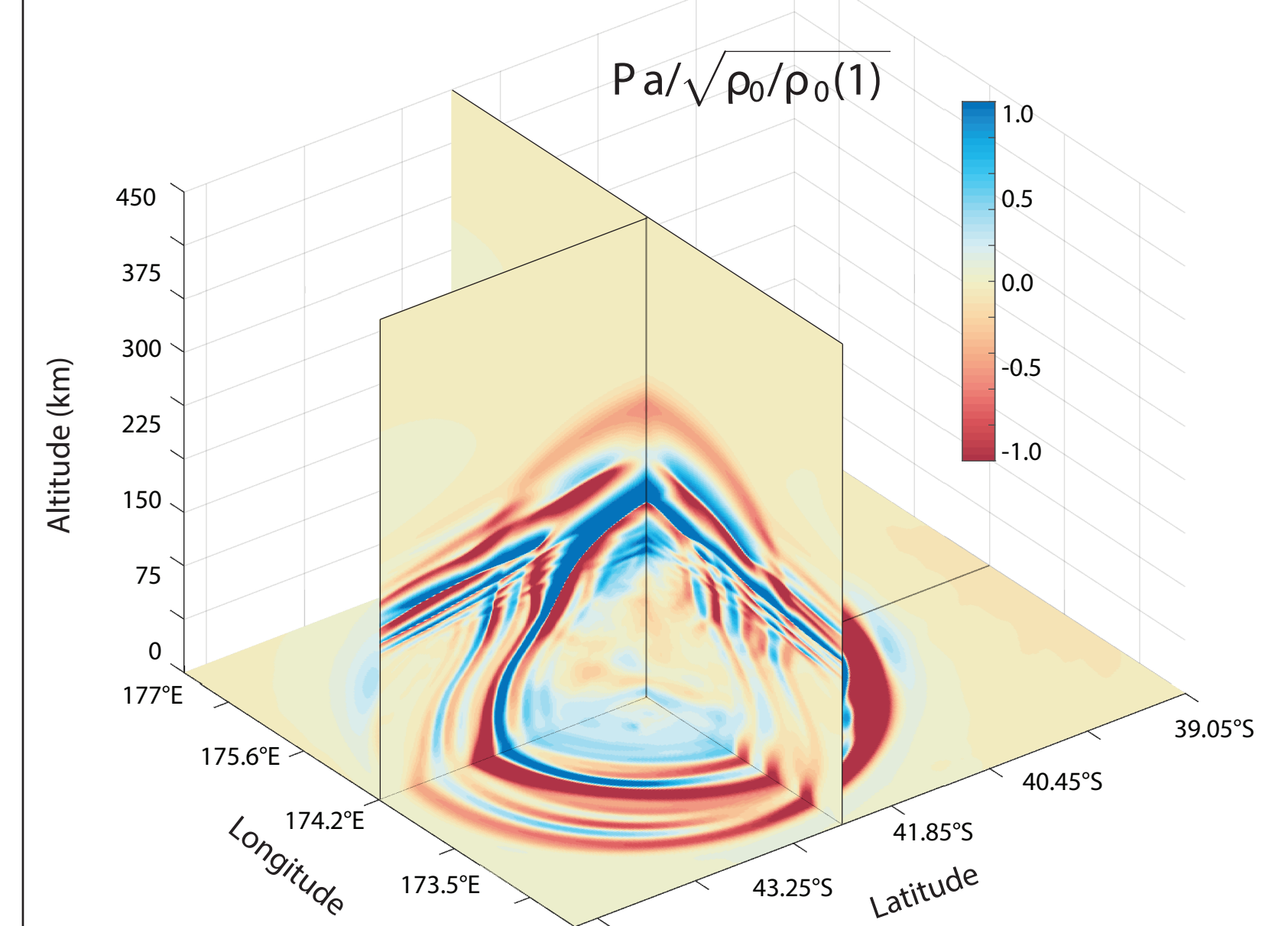
Observations

Coseismic Ionospheric Disturbances (CIDs) in Total Electron Content (TEC) measurements were first registered ~8-10 min after the earthquake that is consistent with time of acoustic waves reaching ionospheric F-layer. Stronger CIDs are observed to the north from the epicenter, that is connected with dominant electron mobility along magnetic field lines. Apparent phase velocity of CIDs is ~0.8-1.1 km/s. Second and third packets of AWs driven CIDs are seen ~15-20 and ~45-55 min later, respectively. The source of these CIDs are reflected back/forth AWs between surface/troposphere and thermosphere. We did not find any additional source of these CIDs as proposed in (Li et al., 2018). Observed CIDs were up to ~5% from the background electron density (0.5 TECu). No signatures of tsunami driven AGWs were found in TEC.

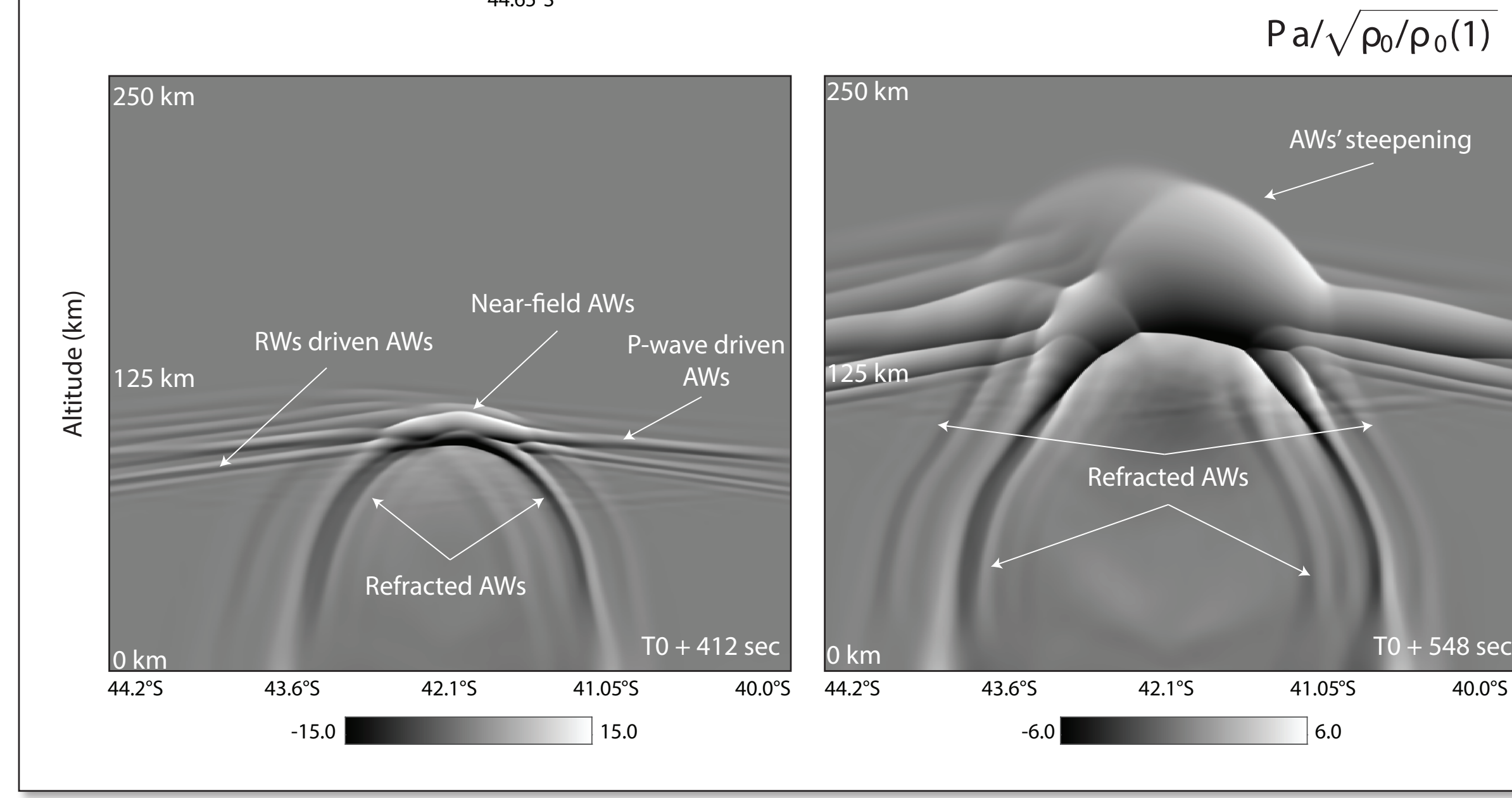


Observed and modeled vTEC are compared for satellite-stations pairs with similar geometry for GPS PRN 20, 75-90° elevation angle and +/-15° from meridional direction 173°E (b). Modeled vTEC is vertically integrated electron density along 172.52°E (d).

Neutral Atmosphere Simulation Results

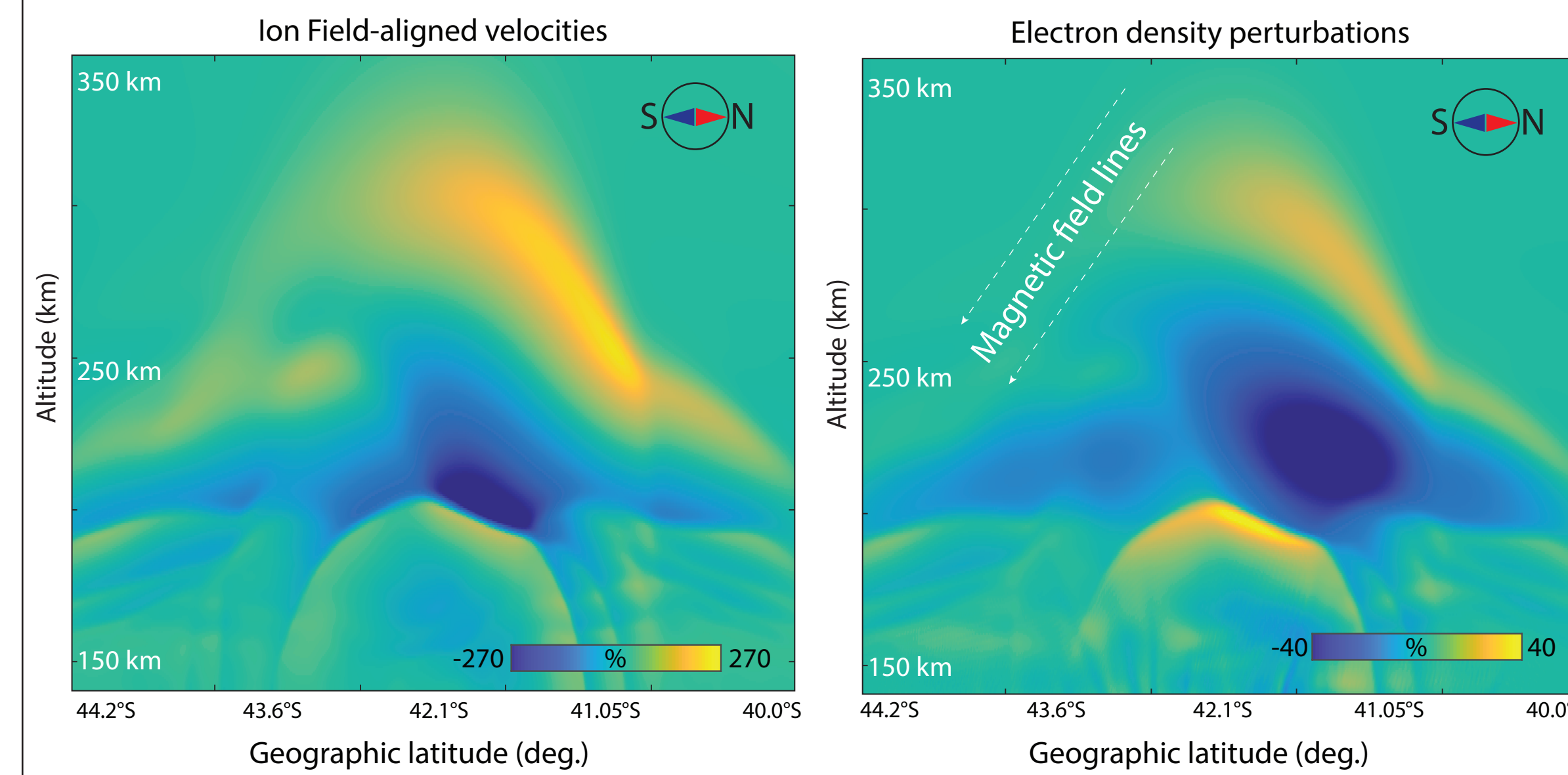


Simulation results show that strong nonlinear AWs were excited by permanent displacements from focal area region. AWs driven by body and surface seismic waves, farther from epicenter, are also presented and propagate in linear regime. Refraction of AWs, both at stratospheric heights (~50 km) and at mesopause (~90-120 km), occurs. Increasing of amplitudes and steepening of AW fronts can be seen from the lower thermosphere, up to ~270 km. At higher altitudes, dissipation mechanisms start leading to the attenuation and smoothing of the AWs. Later in time, the acoustic resonances, generated by trapping of AWs between lower thermosphere and troposphere/surface are presented.



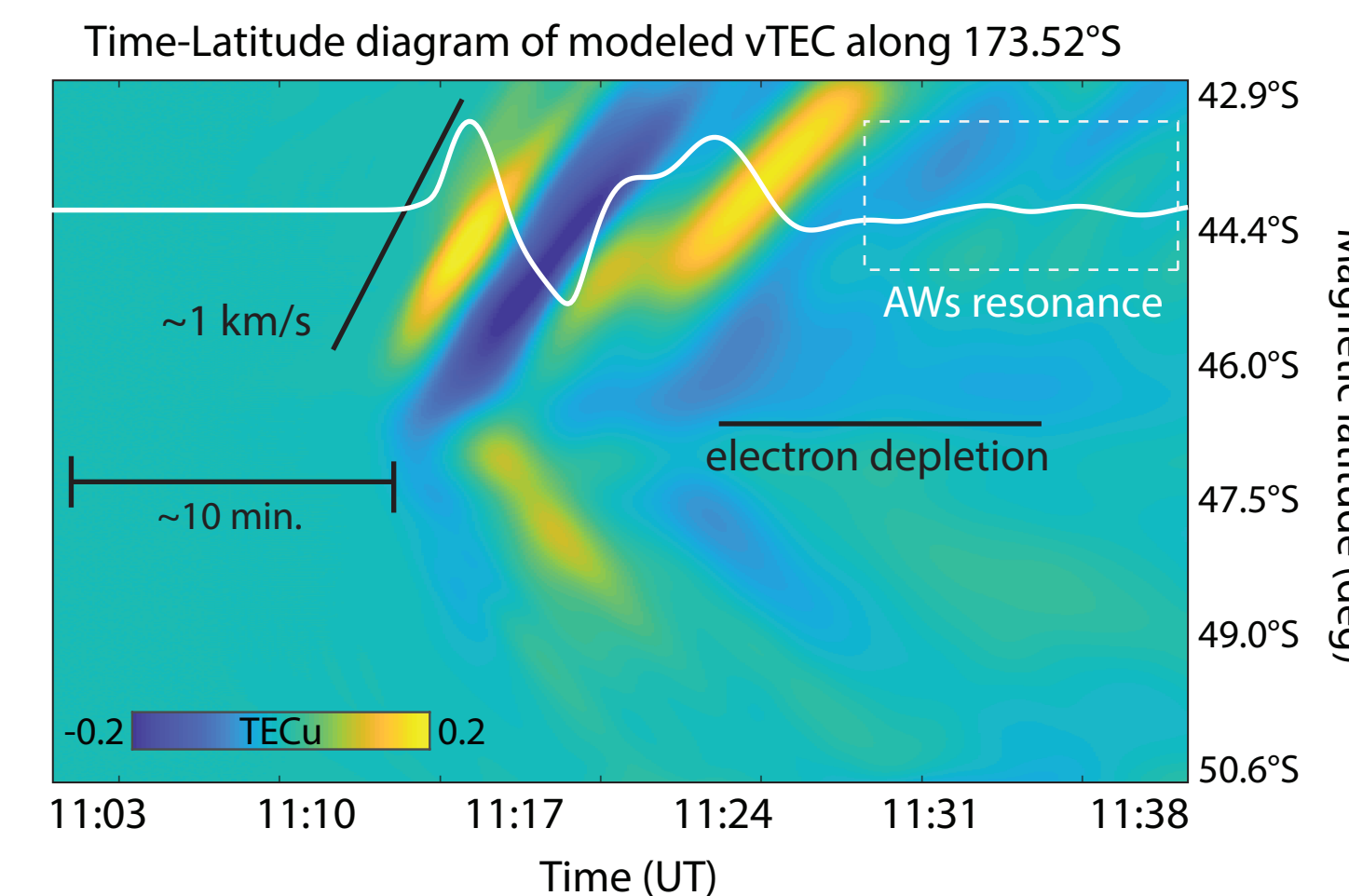
Ionospheric Responses to AWs

Densities of O, N₂, O₂, vertical and meridional velocities, and temperature perturbation data are sent from MAGIC to GEMINI time-dependently to simulate ionospheric response based on chemistry, collisions, drag and dynamic electric fields production. Modeled ion field-aligned velocity and electron density perturbations (in % from the background) driven by the propagation of AWs is presented at the figure below. Ion field-aligned drift velocity is a density weighted value of six ion species velocities. As it was shown in (Zettergren & Snively, 2015), the plasma motion for altitudes lower than ~350 km is driven mostly by directly-forced perturbations from the neutral gas. The strongest perturbations in ionospheric plasma are observed above the epicentral area and driven by permanent displacements' excited AWs. The perturbations driven by AWs excited by surface Rayleigh waves are also seen, but exhibit comparatively negligible amplitudes.



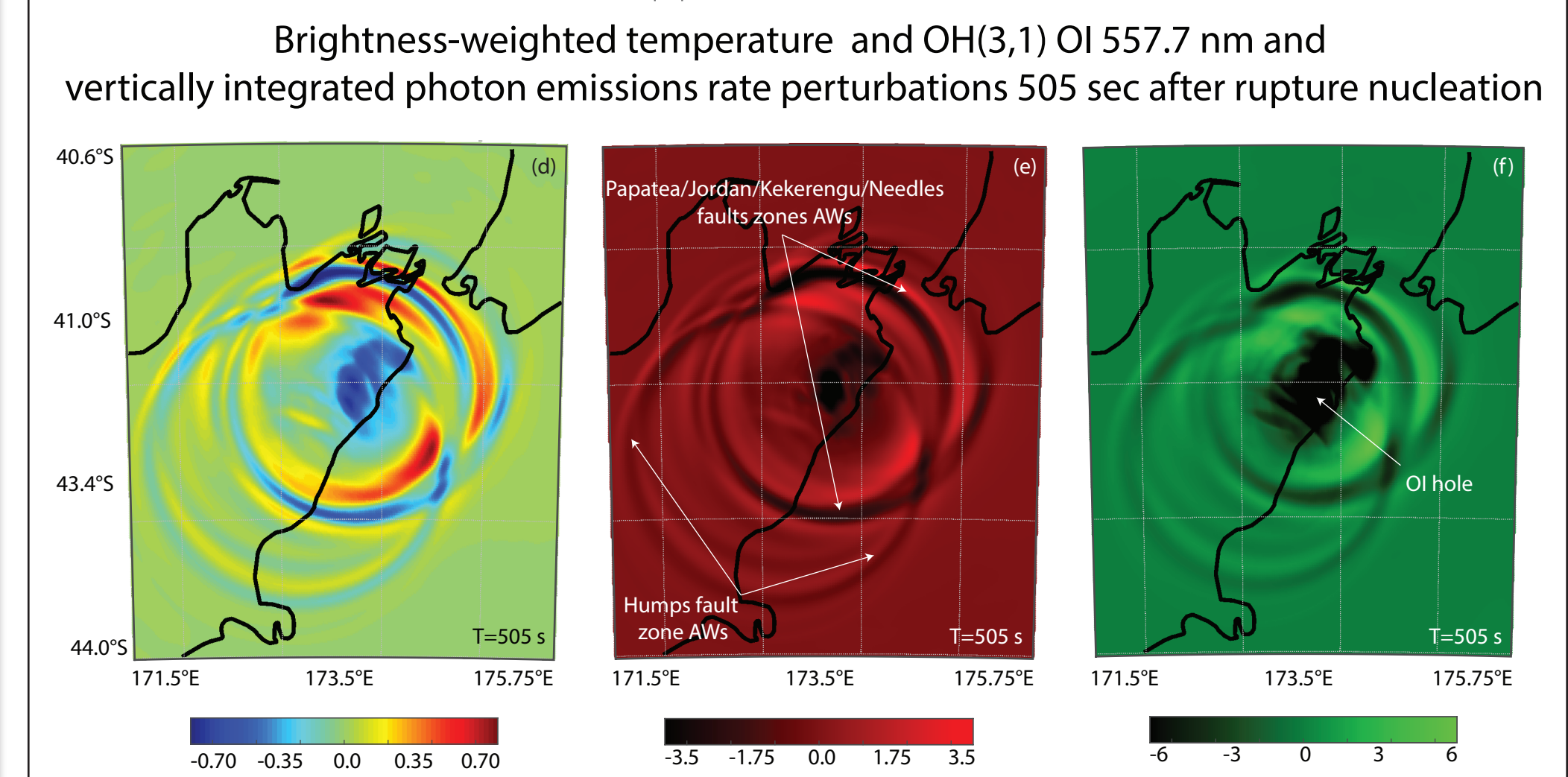
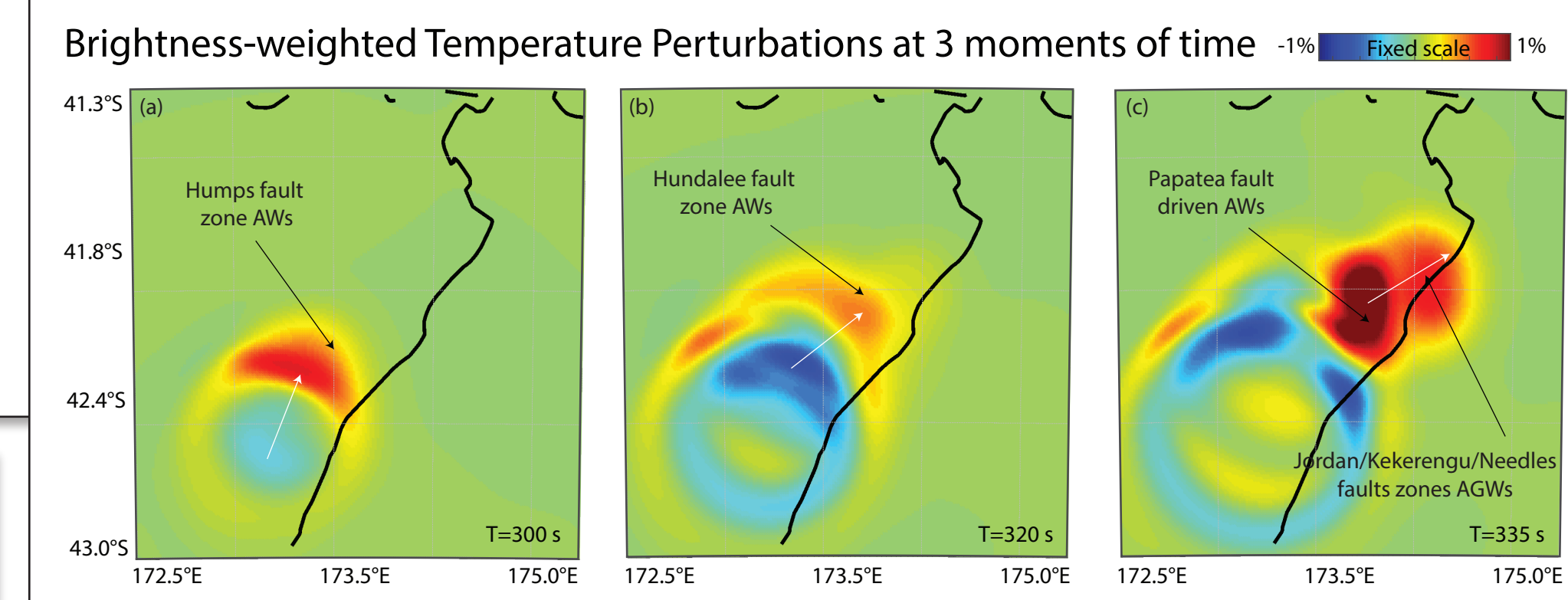
Plasma responses by transport of charged particles confined predominantly along magnetic field lines, which are inclined towards the local zenith direction equator-wardly. The directivity of AWs to north also contributes to higher perturbations to south. Vertically integrated modeled electron density (that corresponds to 90° elevation angle line-of-sight) are presented on the figure below. The azimuthal asymmetry of perturbations can be clearly seen. Above the epicenter fairly small perturbations are observed what points to the importance of LOS direction. First detectable perturbations appeared 10 minutes after rupture nucleation. Apparent speed of CID propagation is ~0.9-1 km/s that corresponds to the speed on sound in ionosphere. Fairly negligible depletion is observed above the epicenter and recovers in ~35 min. The frequency of CIDs are ~3.5 min.

Future works need to include the investigation of full 3D earthquake-ionosphere coupling processes through the coupling of 3DMAGIC-3DGEMINI models. This will particularly allow us to track satellite-station pairs and calculate TEC along realistic LOS. However, the amplitudes, velocities, periods and pattern (as show in observation section) shows fairly good agreement with TEC observations.



Mesospheric Airglow Perturbations Simulation

Hydroxyl OH(3,1) band (~1.5μ) and OI (557.7 nm) mesosphere airglow (MA) perturbations, driven by coseismic AWs, are simulated. The dynamics and chemistry for minor species, OH(3,1) and OI are discussed in (Snively et al., 2010). OH(3,1) brightness-weighted temperature perturbations (panels a-c) for 3 moments of time, along with OH(3,1) and OI vertically integrated photon volume emission rate (zenith observations) and OH(3,1) temperature perturbations at T0+505 sec (panels d-f) are shown on Figure below. T0 is rupture nucleation time.



MA observations could help to track spatial and temporal dynamics of earthquake, starting at Humps fault zone (a), then at Hundalee fault zone (b) and finally at Papatea, Kekerengu and Needles faults zone (c). Two main zones of AWs excitation are clearly seen (panels d-f), that is in agreement with maximum vertical displacements at the surface at these zones. Maximum intensity perturbations are up to 8% and 6% in OH(3,1) and OI photon emission rates, respectively.

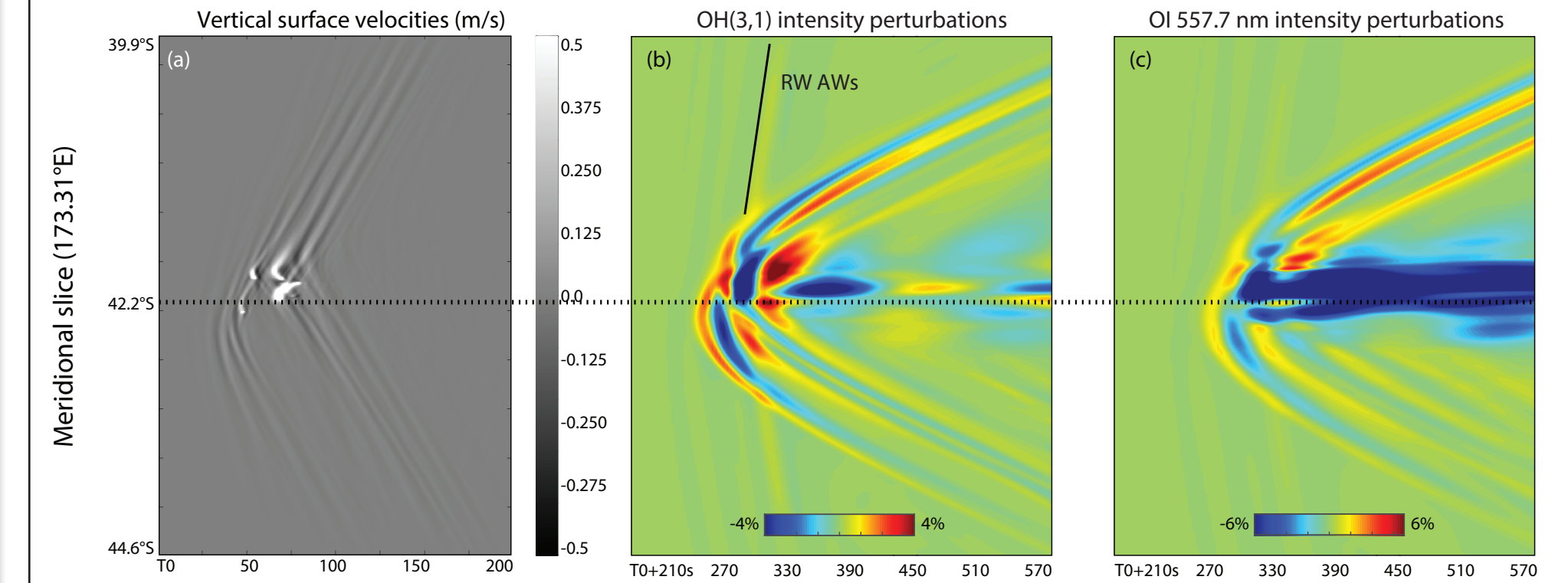


Figure above presents zonal of meridional slices of vertically integrated photon emission rate of OH(3,1), OI and OH(3,1) intensity perturbations, along with surface vertical velocities. Strong perturbations driven by near-field AWs, as well perturbations driven by Rayleigh waves' AWs are detectable. The depletion in OI is up to 14%, after shock AWs arrival from Papatea fault.

Conclusion

Through the analysis of presented modeling results, several important outcomes can be highlighted: 1) weak background electron density results in small perturbations in plasma (in absolute values), even driven by strong shock AWs; 2) mesospheric airglow observations may supplement seismological studies (particularly for complex earthquakes) and improve earthquake-atmosphere-ionosphere coupling processes studies; 3) the AW resonances can be detected an hour after the earthquake; 4) the direction of rupture propagation plays an important role in the spatial distribution of mesospheric and ionospheric perturbations.

Acknowledgements
 This research was supported by NASA grant NNX14AQ39G to ERAU and NNH15ZDA001N-ESI via subcontract from JPL and NSF CAREER awards (Snively's) and (Zettergren's). We acknowledge the New Zealand GeoNet project and its sponsors EQC, GNS Science and LINZ, for providing GNS data used in this study. We thank Ian Hamling for providing us the vertical displacement field derived from SAR azimuth and range offsets. The authors gratefully acknowledge the use of the ERAU Vega High-Performance Computing Cluster.